Materials Science in Semiconductor Processing 63 (2017) 6–11

Contents lists available at ScienceDirect

Materials Science in Semiconductor Processing

journal homepage: www.elsevier.com/locate/mssp

# Enhanced photocatalytic activity of water stable hydroxyl ammonium lead halide perovskites

Muhammad Aamir[a], Zawar Hussain Shah[b], Muhammad Sher[a], Azhar Iqbal[b], Neerish Revaprasadu[c], Mohammad Azad Malik[d], Javeed Akhtar[e,*]

[a] Department of Chemistry, Allama Iqbal Open University, Islamabad, Pakistan
[b] Department of Chemistry, Quaid-i-Azam University, Islamabad, Pakistan
[c] Department of Chemistry, University of Zululand, Private Bag X1001, KwaDlangezwa 3880, South Africa
[d] School of chemistry & materials science centre, The university of Manchester, Oxford Road, M13 9PL United Kingdom
[e] Department of physics, polymers & materials synthesis (PMS) Lab Nanoscience and Materials Synthesis Lab (NMSL), COMSATS, Institute of Information Technology (CIIT), Chak Shahzad, Islamabad, Pakistan

ARTICLE INFO

*Keywords:*
Pervoskite
Solar cell
Thin films
Photocatalysis

ABSTRACT

Hybrid perovskite have shown a potential as structurally and chemically tunable materials with interesting optical properties. Herein, We describe the synthesis and characterization of two new perovskites, hydroxyl ammonium lead iodo chloride, $OHNH_3PbI_2Cl$ **(1)** and hydroxyl ammonium lead chloride, $OHNH_3PbCl_3$ **(2)** by wet-chemical route. The as-prepared **(1)** and **(2)** have shown promising optical properties with suitable band gaps 3.7 eV and 3.9 eV respectvely. Time resolved Photoluminescence (PL) results showed that hybride pervoskite **(2)** had a long lived PL whereas **(1)** exhibited a short PL life-time. Thermo-gravimetrical analysis (TGA) in nitrogen gas environment revealed that **(1)** and **(2)** are stable and do not show any sign of decomposition up to ~200 °C. Photocatalytical performance of as-prepared materials **(1)** and **(2)** under sunlight were mointerted using textile dye direct yellow. The compound **(1)** degraded dye in 20 min while **(2)** in 55 min with superior recyclablity.

## 1. Introduction

Organic-inorganic hybrid perovskites are a new class of materials which have received considerable interest across the spectrum of physical sciences due to their novel and enhanced optoelectronic properties.[1,2] Amongst the solar light absorbing materials, hybrid perovskites have attained promising attention, because of their facile synthesis, less toxicity and easy processing.[3,4] They have superseded the use of traditional dyes sensitized solar cells by absorbing across a wide range of the solar spectrum showing device efficiency over 20%. [5] The tunable band gap, high absorption/optical coefficient, and extraordinary charge carrier mobility are the important properties that make them potentially useful candidates for photovoltaic applications. [6–8] Structurally, organic-inorganic hybrid perovskite have $ABX_3$ stoichiometry, where, (A=small organic cation, B=divalent metal cation, X=halogen), $BX^{6-}$ anion forms octahedral geometry with A component neutralizing the charge and fill the interstices.[4,9] [10] The spherical (e.g. inorganic) to non-spherical (e.g. organic or inorganic) A site component provide a basis to clearly distinguish between hybrid and inorganic perovskites.[10] The choice of a wide variety of organic and inorganic counterparts of perovskite can tailor electrical, mechanical, magnetic and optical properties. Therefore they have been considered suitable candidates for high efficacy solar devices, [11–16] light emitting diodes [17] and sensors.[18,19] However, organic cations impart moisture and thermal instability.[4, 20–22] These stability parameters are critical for the optoelectronic performance of devices. Various attempts have been made to improve the stability of hybrid perovskites by modifying the organic cation or halide ions. But, the effects of these measures were modest because of structure distortion and weak interaction between the organic and inorganic components.[23,24].

The industrial effluent contains a substantial amount of organic dyes which pose serious threat to aquatic life. [25,26] Degradation of such toxic dyes has been attempted by the use of ZnO,[27,28] $TiO_2$, [29,30] CuO [31,32] nanostructures. However, they need ultraviolent radiations to start degradation reaction, thus limiting their large scale use.[33–36] Further, due to nano size, the disposal of these materials needs special methods.[37–39] Pervoskite materials have superior visible light absorbing capacity.[25, 26, 40–42] Therefore, perovskites have a potential to be used as photocatalyst to degrade toxic wastes.

* Corresponding author.
*E-mail address:* javeedk@comsats.edu.pk (J. Akhtar).

http://dx.doi.org/10.1016/j.mssp.2017.01.001
Received 3 August 2016; Received in revised form 26 November 2016; Accepted 2 January 2017
Available online 27 January 2017

In this work, we report the preparation of new hydroxyl ammonium lead halide perovskites **(1)** and **(2)**, using hydroxylamine precursor-an important intermediate in biological nitrification process,[43] instead of traditionally used organic moiety. The as-prepared compounds **(1)** and **(2)** were characterized by powdered X-ray diffraction (*p*-XRD), ultraviolent/visible spectroscopy (UV–Vis), steady state photoluminescence spectroscopy (SPL) and time resolved photoluminescence (TRPL). Further, the stability of as-synthesized compounds **(1)** and **(2)** was investigated in aqueous medium. The thermal stability was studied by thermal gravimetrical analysis (TGA/DTA) followed by visible light driven photocatalysis under ambient conditions. To the best of our knowledge, this aspect of prepared perovskite **(1)** and **(2)** have not been reported in the literature.

## 2. Experimental section

### 2.1. Materials

Hydroxyl ammonium chloride ($OHNH_3^+Cl^-$), lead chloride ($PbCl_2$), lead iodide ($PbI_2$) and anhydrous DMF were purchased from Sigma-Aldrich and used without further purification.

### 2.2. Characterization

Phase purity of synthesized materials were confirmed by powdered X-ray diffraction using X' Pert PRO PANalytical equipment with Cu Kα radiation (K=1.54178).

UV–Vis spectra were measured by using Shimadzu UV-1700 spectrophotometer at room temperature. The PL life-time was measured by using the standard instrument Flau Time 300 (FT-300) steady state and life-time spectrometer, PicoQuant GmbH, Germany. Thermal stability was tested by Shimadzu DTG-60/DTG-60A.

### 2.3. Synthesis of $OHNH_3PbI_2Cl$ perovskite (1)

Hydroxyl ammonium lead iodo chloride ($OHNH_3PbI_2Cl$) **(1)** was synthesized by treating 14 mmole of hydroxyl ammonium chloride ($OHNH_3^+Cl^-$) and 14 mmole of $PbI_2$ in DMF (10 $cm^3$) solvent at 80 °C for 12 h with stirring. The reaction mixture was kept at room temperature for two weeks. The pale yellow coloured crystals were than filtered and dried at room temperature.[44].

### 2.4. Synthesis of $OHNH_3PbCl_3$ perovskite (2)

The synthesis of hydroxyl ammonium lead chloride ($OHNH_3PbCl_3$) **(2)** was carried out by reacting 14 mmole of hydroxyl ammonium chloride ($OHNH_3^+Cl^-$) with 14 mmole of $PbCl_2$ in 10 $cm^3$ of DMF at 80 °C for 2 h with stirring. The white crystalline powder was formed which was filtered and dried at room temperature.[44].

### 2.5. Procedure for photocatalysis

The photocatalytic activity of as-synthesized hybrid perovskites **(1)** and **(2)** was tested for the degradation of dye Direct Yellow 27. For the reproducibility of results all experiments were conducted under similar conditions. The degradation experiment was performed under natural light using same procedure as reported in literature.[45,46] The photodegradation experiment was carried out by adding 20 mg of synthesized hybrid perovskite in 40 ml of 5 ppm aqueous dye solution with initial concentration of 2 mg/ml. The reaction mixture was stirred in dark for 15 min at room temperature. The suspended catalyst was allowed to settle down by keeping the reaction mixture at room temperature for 10 min. The dye concentration was measured by UV–Vis spectroscopy. The reaction mixture was placed in sunlight at ambient laboratory condition and the samples were withdrawn after fixed time intervals to measure the concentration of dye until the complete degradation of dye.

### 2.6. Procedure for COD

The concentration of dye in the sample before and after the treatment with as-synthesized compounds **(1)** and **(2),** the COD experiment was performed by taking 50 ml of the sample into a 500 ml refluxing flask. Added 1 g of $HgSO_4$ and 5 ml of sulphuric acid reagent (5.5 g of $Ag_2SO_4$ per kg of concentrated $H_2SO_4$) and stirred the mixture till dissolution of $HgSO_4$. Then add 25 ml of 0.042 M $K_2Cr_2O_7$ solution and mixed well. To the resultant solution 70 ml of sulphuric acid reagent was added with stirring and allowed the mixture to reflux for two hours. Cooled and washed the condenser and collected the material. The volume of the sample was doubled by addition of distilled water and cooled the material to room temperature. Excess amount of $K_2Cr_2O_7$ was determined with Ferrous Ammonium Sulphate (FAS) titration using few drops of ferroin indicator. The end point indicated by colour change from blue green to reddish brown that persisted for more than one minute.[25,47].

The same procedure was repeated for blank sample using Deionized water as a sample COD value was calculated using following formula.

$$COD\ (mg\ O_2/L)=\frac{(A-B)\times M\times 8000}{V_s}$$

A=Volume of FAS used for blank in ml.

B=Volume of FAS used for sample in ml.

$V_s$=Volume of sample in ml.

M=Molarity of FAS solution.

## 3. Results and discussion

Hybrid perovskites **(1)** and **(2)** were prepared by a solution method.[44] The precursor hydroxyl ammonium chloride and lead halide were stirred at 80 °C. The reaction of compound **(1)** completed in 12 h while **(2)** in 2 h. Compound **(1)** and **(2)** were crystalized in DMF solvent at room temperature. Compound **(1)** gave yellow coloured crystals while **(2)** gave a white product. The powdered X-ray diffraction (p-XRD) showed that **(1)** and **(2)** have perovskite structure. Both compounds give sharp peaks indicating the highly crystalline nature of products. Fig. 1 shows that compound **(1)** have tetragonal peak pattern while compound **(2)** gave hexagonal pattern. Similar results are also reported in the literature.[48,49] Fig. 2(a) Shows the absorbance spectra of $OHNH_3PbI_2Cl$ **(1)** and $OHNH_3PbCl_3$ **(2)** measured at room temperature in DMF. The sharp absorption peaks of **(1)** and **(2)** indicate that these hybrid perovskites have direct band gaps which were calculated by using Tauc equation. The estimated band gap for $OHNH_3PbI_2Cl$ **(1)** is 3.7 eV and for $OHNH_3PbCl_3$ **(2)** is 3.9 eV. The data shows that the band gap decreases from 3.9 to 3.7 eV by the incorporation of iodine in the hybrid perovskites. The direct band gaps of hybrid perovskite semiconductors **(1)** and **(2)** predict that they could be potential candidates

**Fig. 1.** *p*-XRD spectra of synthesized hydroxyl ammonium lead halides **(1)** and **(2).**

**Fig. 2.** UV-Vis spectra of synthesized Hydroxyl Ammonium Lead Halides **(1)** and **(2)** with Inset showing the tauc plot of **(1)** and **(2)**.

for photocatalysis and photovoltaic applications. However, indirect band gaps of as-prepared compounds was also measured. The estimated indirect band gaps were found to be 3.5 eV for **(1)** and 3.8 eV for **(2)**.

### 3.1. Photoluminescence (PL) properties

The steady-state photoluminescence is presented in Fig. 3(a). Both the compounds **(1)** and **(2)** emit in the visible region. Compound **(1)** shows three PL features at 414 nm, 531 nm and 610 nm following excitation at 306 nm. By incorporating iodine in the perovskite structure, slightly red shift in the PL spectra is observed (Fig. 3(a), red trace). The three peaks in the PL spectra of each compound **(1)** and **(2)** suggest the existence of at least three distinct emissive states [50]. The samples of the compounds **(1)** and **(2)** were excited with a pulsed LED laser at 306 nm. The time-resolved PL of both the compounds was measured by selecting the PL at peak locating at 414 nm. Compound **(2)** showed a very long lived PL that persists up to 100 ns and the measured experimental PL was best fitted by tri-exponential decay function (Fig. 3b, solid green trace) suggesting the time constants of $\tau_1$=1.408 ns ± 0.042 ns, $\tau_2$=7.141 ns ± 0.157 ns, $\tau_3$=63.382 ns ± 0.305 ns. While compound **(1)** showed a very short PL life-time and the measured PL was also best described by tri-exponential decay function (Fig. 3b, solid red trace) with time constants of $\tau_1$=1.045 ns ± 0.017 ns, $\tau_2$=4.128 ns ± 0.030 ns, $\tau_3$=12.487 ns ± 0.051 ns. Fitting the experimental data with tri-exponential decay function suggest that the PL is originating at three distinct states. This observation is also in consistent with stead-state PL (Fig. 3a), where three distinct PL features have been observed. The longer PL life time may be due to long diffusion length of as-synthesized hybrid perovskite **(2)** and may provide an evidence of having good photovoltaic performance. The blue trace in Fig. 3(b) represents the instrument response (IR) function of the instrument with full width half maximum (FWHM) ~500 ps, indicating that the PL of the compounds **(1)** and **(2)** can easily be resolved and measured. The difference in the PL life-time of compounds **(1)** and **(2)** indicates that the fluorescing states have completely different environments. The quenching of PL in compound **(1)** might occur due to the introduction of states by iodine (I). These states are empty before excitation and the photo-injected electrons might be trapped in these states, as a result we see quenching and shortening of PL. The PL quenching effect in compound **(1)** is also supported by the steady-state PL spectrum, where a slight less PL intensity of compound **(1)** has been observed.

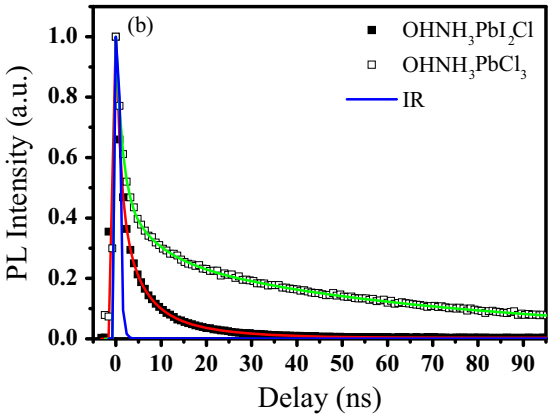


**Fig. 3. (a)** Steady-state photoluminescence spectra of compounds **(1)** and **(2)** after excitation at 306 nm, **(b)** Time-resolved PL kinetics of compounds **(1)** (solid squares and solid red trace represents the fitted model) and **(2)** (open squares and solid green trace represents the fitted model) after pulsed excitation at a wavelength of 306 nm. The solid blue trace represents the instrument response (IR) of the instrument. (For interpretation of the references to color in this figure legend, the reader is referred to the web version of this article.)

### 3.2. Stability studies

To investigate the water stability of the synthesized Hydroxyl Ammonium Lead Halides **(1)** and **(2)**, the respective compounds were added separately in deionized water under stirring for one hour at ambient condition. The deionized water was run in VU-Vis spectroscopy to determine the ion contamination in doubly deionized water and was found that there are no ions in water. It was observed that the colour of hybrid perovskites **(1)** and **(2)** remained unchanged for 45 days. To find out the long term stability of synthesized hybrid perovskites **(1)** and **(2),** the UV–Vis studies were performed. The water mixture of hybrid perovskites was monitored by UV–Vis for 45 days under ambient condition. Fig. S1 (a) and (b) (supplementary information) shows that hybrid perovskites are soluble in water at room temperature. The UV–Vis graph shows that there no shift in absorption band, suggesting that these compounds are water soluble and stable at ambient condition. The stability of as-synthesized hybrid perovskites **(1)** and **(2)** may be due to individual hydrogen bonding formed by the hydroxyl and ammonium parts of inorganic cations.

TGA-DTA measurements on the powdered crystals of synthesized hydroxyl ammonium lead halides **(1)** and **(2)** showed that synthesized hybrid compounds are thermally stable upto 200 °C as shown in the Fig. 4(a) and (b). The compound **(1)** shows weight loss 8.71% at 57 °C that represent the removal of water and organic solvent. The calculated weight loss 9.43% at 220 °C is showing the removal of $OHNH_3Cl$ component from the hybrid perovskites. The residual weight was found to be near to that expected for Lead (II) Iodide. On the other hand, hybrid perovskite **(2)** is comparatively more stable as compared to the

**Fig. 4. (a)** TGA and DTA analysis of hybrid perovskites **(a)** for **(1)** and **(b)** for **(2)**.

hybrid perovskite **(1)**. The higher thermal stability of **(2)** as compare to **(1)** could be be due to the size of halides in the as-synthesized hybrid perovskites. Compound **(2)** has chlorides, forming a uniform octahedral geometry of $PbCl_6^-$ anions. While, in the hybrid perovskite **(1)** the octahedral geometry formed by the $PbI_4Cl_2^-$ may be non-uniform because of the size difference in the iodide and chloride ions. The weight loss (about 8.18%) of the hybrid perovskite **(2)** after 200 °C suggested the loss of $OHNH_3Cl$. The residual weight is an indication of $PbCl_2$. DTA analysis of compound **(1)** shows four distinct endothermic peaks ranging from 350 °C to 500 °C, on the other hand, compound **(2)** shows two endothermic peaks at 200 °C and 300 °C which may indicate the change in phases and decomosition of perovskites as shown in Fig. 4(a) and (b).

### 3.3. Photocatalysis of as-prepared Perovskites

Fig. S2 (a) and (b) (supplementary information) shows the successive degradation of 5 ppm aqueous solutions of Direct Yellow by $OHNH_3PbI_2Cl$ **(1)** and $OHNH_3PbCl_3$ **(2)** photocatalysts. It was found that the catalyst **(1)** takes 20 min while **(2)** takes 55 min to degrade the aqueous solution of direct yellow. The difference in degradation time may be observed due to difference in direct band gap of catalysts. The blank dye solution was also placed in sunlight under the same condition, to observe the dye degration rate without catalyst as shown in Fig. S2 (c) which suggests that no significant dye degradation takes place in the absence of catalyst. Fig. 5 shows the % degradation of dye with time. In the first experiment, the 5 ppm dye solution having catalyst **(1)** under sunlight, showed 38.08% degradation in first 5 min.. After 20 mints under sunlight, the catalyst **(1)** drives 93.98% dye degradation. In the second experiment, the catalyst hydroxyl ammonium lead chloride **(2)** was added to the 5 ppm aqueous solution of dye under sunlight. It was noted that the 82.19% dye degrade in the first five minutes. Afterward the degradation rate in both experiments slowed down because the concentration of dye drops significantly that lower the rate of collision of dye molecules with the radicals.

**Fig. 5.** %age degradation of direct yellow Dye in the presence of **(1)** and **(2)**.

**Fig. 6.** Degradation time and % degradation at various dye concentrations.

Initial concentration of dye in the degradation experiment is an important factor as dye concentration varies in the industrial wastewater. It is observed that the % degradation of dye decreases as the dye concentration increases by keeping a fixed amount of catalyst. [51] It is due to that the more dye molecules are adsorbed at the surface of catalyst so less photons reaches the catalyst. Therefore, fewer electrons ejected from the catalyst surface leading to drop in % degradation with increase in degradation time. [52].

Fig. 6 shows the effect of initial dye concentration ranging from 5 to 30 ppm on photodegradation of dye. It was found that the time required for dye degradation also increases as the concentration of dye increases from 5 ppm to 30 ppm having fix amount of respective catalysts. It is a fact that as the dye concentration increases the colour of solution becomes more intense, which may be the reason of the low degradation efficiency of the catalyst. The % degradation of various dye concentrations (5–30 ppm) in the first 5 min of irradiation under the sun in the presence of fixed amount of respective catalysts have also shown that increasing the dye concentration drops the photodegradation ability of catalysts due to saturation point. The catalysts **(1)** and **(2)** were successfully separated and reused for five times. The catalytic ability of **(1)** and **(2)** remained same throughout in repeated experiments.

The large band gap semiconductors have been widely used for the degradation of effluents.[53–55] It has been reported that the trap states in the wide band gap semiconductors like ZnS, [56] $Sr_2Sb_2O_7$, [54] etc are responsible for dye degradation because these absorb the visible light spectrum.[57] Therefore, it is suggested that the compounds **(1)** and **(2)** also shows that same behaviour because of trap states produced by the aerial oxygen and nitrogen that are mixed during the reaction. On the basis of literature,[57,58] the possible mechanism for the dye degradation over the compounds **(1)** and **(2)** can be proposed in Scheme 1. To find out the adsorption and degradation of dyes, the COD measurement were performed on the solution. Fig. S3 shows that the small change in COD (about 20%) that attributes that small amount of dye is adsorbed on the surface of compounds **(1)** and **(2)**. The change in concentration of dye before and

**Scheme 1.** Proposed mechanism for the degradation of dye direct yellow 27 using as-prepared compounds **(1)** and **(2)**.

after irradiation in the presence of catalysts provides an evidence for dye degradation.

## 4. Conclusions

In conclusion, the present work describes the successful synthesis of hydroxyl ammonium lead halides **(1)** and **(2)** by wet chemical method. The *p*-XRD spectrum confirms the crystalline nature of hybrid perovskites. The TRPL analysis reveals that the PL life time of **(1)** is short as compare to **(2)**. The 3.7 eV and 3.9 eV are band gaps suggests these compounds have good light harvesting ability. In addition, the as-synthesized compounds **(1)** and **(2)** are thermally stable up to 200 °C and water stable for 45 days. The hybrid perovskites **(1)** and **(2)** have shown promising photocatalytic ability. The water stability of as-synthesized compounds **(1)** and **(2)** provide a basis to be used these compounds in solar cells. Further, work is in progress to test and optimise their light harvesting property in solar cells.

## Acknowledgements

The authors greatly acknowledge financial assistance from Higher Education Commission (HEC) (Project #20-3020/R & D/HEC/14/654). JA thanks COMSATS institute of information technology for providing start-up grant. N.R. acknowledges the National Research Foundation (South Africa) (Grant #64820 (SARChi)) for funding. MA acknowledges the University of Manchester for funding.

## Appendix A. Supplementary material

Supplementary data associated with this article can be found in the online version at http://dx.doi.org/10.1016/j.mssp.2017.01.001.

## References

[1] A. Kojima, K. Teshima, Y. Shirai, T. Miyasaka, Organometal halide perovskites as visible-light sensitizers for photovoltaic cells, J. Am. Chem. Soc. 131 (2009) 6050–6051.
[2] H.J. Snaith, Perovskites: the emergence of a new era for low-cost, high-efficiency solar cells, J. Phys. Chem. Lett. 4 (2013) 3623–3630.
[3] M.A. Green, A. Ho-Baillie, H.J. Snaith, The emergence of perovskite solar cells, Nat. Photonics 8 (2014) 506–514.
[4] J.M. Frost, K.T. Butler, F. Brivio, C.H. Hendon, M. Van Schilfgaarde, A. Walsh, Atomistic origins of high-performance in hybrid halide perovskite solar cells, Nano Lett. 14 (2014) 2584–2590.
[5] P. Gao, M. Grätzel, M.K. Nazeeruddin, Organohalide lead perovskites for photovoltaic applications, Energy Environ. Sci. 7 (2014) 2448–2463.
[6] W.J. Yin, T. Shi, Y. Yan, Unique properties of halide perovskites as possible origins of the superior solar cell performance, Adv. Mater. 26 (2014) 4653–4658.
[7] C. Wehrenfennig, G.E. Eperon, M.B. Johnston, H.J. Snaith, L.M. Herz, High charge carrier mobilities and lifetimes in organolead trihalide perovskites, Adv. Mater. 26 (2014) 1584–1589.
[8] D.J. Lewis, P. O'Brien, Ambient pressure aerosol-assisted chemical vapour deposition of (CH 3 NH 3) PbBr 3, an inorganic–organic perovskite important in photovoltaics, Chem. Commun. 50 (2014) 6319–6321.
[9] G.E. Eperon, S.D. Stranks, C. Menelaou, M.B. Johnston, L.M. Herz, H.J. Snaith, Formamidinium lead trihalide: a broadly tunable perovskite for efficient planar heterojunction solar cells, Energy Environ. Sci. 7 (2014) 982–988.
[10] Q. Chen, N. De Marco, Y.M. Yang, T.-B. Song, C.-C. Chen, H. Zhao, Z. Hong, H. Zhou, Y. Yang, Under the spotlight: the organic–inorganic hybrid halide perovskite for optoelectronic applications, Nano Today 10 (2015) 355–396.
[11] F. Wang, H. Yu, H. Xu, N. Zhao, HPbI3: a new precursor compound for highly efficient solution-processed perovskite solar cells, Adv. Funct. Mater. (2015).
[12] C.C. Stoumpos, L. Fraser, D.J. Clark, Y.S. Kim, S.H. Rhim, A.J. Freeman, J.B. Ketterson, J.I. Jang, M.G. Kanatzidis, Hybrid germanium iodide perovskite semiconductors: active lone pairs, structural distortions, direct and indirect energy gaps and strong nonlinear optical properties, J. Am. Chem. Soc. (2015).
[13] H.S. Jung, N.G. Park, Perovskite solar cells: from materials to devices, Small 11 (2015) 10–25.
[14] B. Hailegnaw, S. Kirmayer, E. Edri, G. Hodes, D. Cahen, Rain on methylammonium-lead-iodide based perovskites: possible environmental effects of perovskite solar cells, J. Phys. Chem. Lett. (2015).
[15] H.H. Fang, R. Raissa, M. Abdu-Aguye, S. Adjokatse, G.R. Blake, J. Even, M.A. Loi, Hybrid perovskites: photophysics of organic–inorganic hybrid lead iodide perovskite single crystals, Adv. Funct. Mater. 25 (2015) (Adv. Funct. Mater. 16/2015) (2346–2346).
[16] P.P. Boix, S. Agarwala, T.M. Koh, N. Mathews, S.G. Mhaisalkar, Perovskite solar cells: beyond methylammonium lead iodide, J. Phys. Chem. Lett. 6 (2015) 898–907.
[17] Y.H. Kim, H. Cho, J.H. Heo, T.S. Kim, N. Myoung, C.L. Lee, S.H. Im, T.W. Lee, Light-emitting diodes: multicolored organic/inorganic hybrid perovskite light-emitting diodes, Adv. Mater. 27 (2015) (Adv. Mater. 7/2015)(1303–1303).
[18] K. Hosono, I. Matsubara, N. Murayama, S. Woosuck, N. Izu, Synthesis of polypyrrole/MoO3 hybrid thin films and their volatile organic compound gas-sensing properties, Chem. Mater. 17 (2005) 349–354.
[19] M. Aamir, M. Sher, M.A. Malik, N. Revaprasadu, J. Akhtar, A facile approach for selective and sensitive detection of aqueous contamination in DMF by using perovskite material, Mater. Lett. 183 (2016) 135–138.
[20] A. Dualeh, N. Tétreault, T. Moehl, P. Gao, M.K. Nazeeruddin, M. Grätzel, Effect of annealing temperature on film morphology of organic–inorganic hybrid pervoskite solid-state solar cells, Adv. Funct. Mater. 24 (2014) 3250–3258.
[21] F. Matsumoto, S.M. Vorpahl, J.Q. Banks, E. Sengupta, D.S. Ginger, Photodecomposition and morphology evolution of organometal halide perovskite solar cells, J. Phys. Chem. C (2015).
[22] B. Philippe, B.-W. Park, R. Lindblad, J. Oscarsson, S. Ahmadi, E.M. Johansson, Hk Rensmo, Chemical and electronic structure characterization of lead halide perovskites and stability behavior under different exposures• A photoelectron spectroscopy investigation, Chem. Mater. 27 (2015) 1720–1731.
[23] J.H. Noh, S.H. Im, J.H. Heo, T.N. Mandal, S.I. Seok, Chemical management for colorful, efficient, and stable inorganic–organic hybrid nanostructured solar cells, Nano Lett. 13 (2013) 1764–1769.
[24] N.J. Jeon, J.H. Noh, W.S. Yang, Y.C. Kim, S. Ryu, J. Seo, S.I. Seok, Compositional engineering of perovskite materials for high-performance solar cells, Nature 517 (2015) 476–480.
[25] C. Sahoo, A. Gupta, A. Pal, Photocatalytic degradation of methyl red dye in aqueous solutions under UV irradiation using Ag+ doped TiO 2, Desalination 181 (2005) 91–100.
[26] S. Song, L. Xu, Z. He, H. Ying, J. Chen, X. Xiao, B. Yan, Photocatalytic degradation of CI direct red 23 in aqueous solutions under UV irradiation using SrTiO 3/CeO 2 composite as the catalyst, J. Hazard. Mater. 152 (2008) 1301–1308.
[27] R. Ullah, J. Dutta, Photocatalytic degradation of organic dyes with manganese-doped ZnO nanoparticles, J. Hazard. Mater. 156 (2008) 194–200.
[28] R. Hong, J. Li, L. Chen, D. Liu, H. Li, Y. Zheng, J. Ding, Synthesis, surface modification and photocatalytic property of ZnO nanoparticles, Powder Technol. 189 (2009) 426–432.
[29] C.-y. Wang, D.W. Bahnemann, J.K. Dohrmann, A novel preparation of iron-doped TiO2 nanoparticles with enhanced photocatalytic activity, Chem. Commun. (2000) 1539–1540.
[30] C. Nasr, K. Vinodgopal, L. Fisher, S. Hotchandani, A. Chattopadhyay, P.V. Kamat, Environmental photochemistry on semiconductor surfaces. Visible light induced degradation of a textile diazo dye, naphthol blue black, on TiO2 nanoparticles, J. Phys. Chem. 100 (1996) 8436–8442.
[31] R. Sankar, P. Manikandan, V. Malarvizhi, T. Fathima, K.S. Shivashangari, V. Ravikumar, Green synthesis of colloidal copper oxide nanoparticles using Carica papaya and its application in photocatalytic dye degradation, Spectrochim. Acta Part A: Mol. Biomol. Spectrosc. 121 (2014) 746–750.
[32] S.S. Lee, H. Bai, Z. Liu, D.D. Sun, Novel-structured electrospun TiO 2/CuO composite nanofibers for high efficient photocatalytic cogeneration of clean water and energy from dye wastewater, Water Res. 47 (2013) 4059–4073.
[33] Y.J. Jang, C. Simer, T. Ohm, Comparison of zinc oxide nanoparticles and its nano-crystalline particles on the photocatalytic degradation of methylene blue, Mater. Res. Bull. 41 (2006) 67–77.
[34] V. Gupta, R. Jain, A. Mittal, M. Mathur, S. Sikarwar, Photochemical degradation of the hazardous dye Safranin-T using TiO 2 catalyst, J. Colloid Interface Sci. 309 (2007) 464–469.
[35] C.G. da Silva, J.L. Faria, Photochemical and photocatalytic degradation of an azo dye in aqueous solution by UV irradiation, J. Photochem. Photobiol. A: Chem. 155 (2003) 133–143.
[36] J. Li, F. Sun, K. Gu, T. Wu, W. Zhai, W. Li, S. Huang, Preparation of spindly CuO micro-particles for photodegradation of dye pollutants under a halogen tungsten

lamp, Appl. Catal. A: Gen. 406 (2011) 51–58.
[37] Z. Yinghuai, S.C. Peng, A. Emi, S. Zhenshun, R.A. Kemp, Supported ultra small palladium on magnetic nanoparticles used as catalysts for suzuki cross-coupling and heck reactions, Adv. Synth. Catal. 349 (2007) 1917–1922.
[38] E.A. Meulenkamp, Synthesis and growth of ZnO nanoparticles, J. Phys. Chem. B 102 (1998) 5566–5572.
[39] P.E. Nolan, A.H. Cutler, D.G. Lynch, Method for Producing Encapsulated Nanoparticles and Carbon Nanotubes using Catalytic Disproportionation of Carbon Monoxide and the Nanoencapsulates and Nanotubes Formed Thereby, in, Google Patents, 1999.
[40] S.B. Gajbhiye, Photocatalytic degradation study of methylene blue solutions and its application to dye industry effluent, Int. J. Mod. Eng. Res. 2 (2012) 1204–1208.
[41] F. Fan, X. Wang, Y. Ma, K. Fu, Y. Yang, Enhanced photocatalytic degradation of dye wastewater using ZnO/Reduced graphene oxide hybrids, fullerenes, Nanotub. Carbon Nanostruct. (2015) (00–00).
[42] N. Muhd Julkapli, S. Bagheri, S. Bee Abd, Hamid, Recent advances in heterogeneous photocatalytic decolorization of synthetic dyes, Sci. World J. 2014 (2014).
[43] G. McCarty, Modes of action of nitrification inhibitors, Biol. Fertil. Soils 29 (1999) 1–9.
[44] J.-H. Im, J. Chung, S.-J. Kim, N.-G. Park, Synthesis, structure, and photovoltaic property of a nanocrystalline 2 H perovskite-type novel sensitizer (CH3CH2NH3) PbI3, Nanoscale Res. Lett. 7 (2012) 1–7.
[45] Y. Mameri, N. Debbache, M. el mehdi Benacherine, N. Seraghni, T. Sehili, Heterogeneous photodegradation of paracetamol using Goethite/H 2 O 2 and Goethite/oxalic acid systems under artificial and natural light, J. Photochem. Photobiol. A: Chem. 315 (2016) 129–137.
[46] M.-C. Roşu, C. Socaci, V. Floare-Avram, G. Borodi, F. Pogăcean, M. Coroş, L. Măgeruşan, S. Pruneanu, Photocatalytic performance of graphene/TiO 2-Ag composites on amaranth dye degradation, Mater. Chem. Phys. 179 (2016) 232–241.
[47] S. Motlagh, J. Pawliszyn, On-line monitoring of flowing samples using solid phase microextraction-gas chromatography, Anal. Chim. Acta 284 (1993) 265–273.
[48] F. Lu, X. Wang, Z. Pan, F. Pan, S. Chai, C. Liang, Q. Wang, J. Wang, L. Fang, X. Kuang, Nanometer-scale separation of d 10 Zn 2+-layers and twin–shift competition in Ba 8 ZnNb 6 O 24-based 8-layered hexagonal perovskites, Dalton Trans. 44 (2015) 13173–13185.
[49] J. Dance, J. Soubeyroux, N. Kerkouri, A. Tressaud, Magnetic-structure of the ferrimagnetic H-6 hexagonal perovskite fluoride RB0. 5CS0. 5COF3, Comptes Rendus de L Academie Des Sciences Serie II, 293, 1981, pp.279–282.
[50] T. PEROVA, Polarization Anisotropy of Photoluminescence from Triphenylamine-based Molecular Single Crystal, 2013.
[51] L. Macedo, D. Zaia, G. Moore, H. de Santana, Degradation of leather dye on TiO 2: a study of applied experimental parameters on photoelectrocatalysis, J. Photochem. Photobiol. A: Chem. 185 (2007) 86–93.
[52] M. Rauf, S.S. Ashraf, Fundamental principles and application of heterogeneous photocatalytic degradation of dyes in solution, Chem. Eng. J. 151 (2009) 10–18.
[53] J. Xu, W. Wang, S. Sun, L. Wang, Enhancing visible-light-induced photocatalytic activity by coupling with wide-band-gap semiconductor: a case study on Bi 2 WO 6/TiO 2, Appl. Catal. B: Environ. 111 (2012) 126–132.
[54] H. Xue, Z. Li, L. Wu, Z. Ding, X. Wang, X. Fu, Nanocrystalline ternary wide band gap p-block metal semiconductor Sr2Sb2O7: hydrothermal syntheses and photocatalytic benzene degradation, J. Phys. Chem. C 112 (2008) 5850–5855.
[55] F. Odobel, Y. Pellegrin, Recent advances in the sensitization of wide-band-gap nanostructured p-type semiconductors. Photovoltaic and photocatalytic applications, J. Phys. Chem. Lett. 4 (2013) 2551–2564.
[56] Y. Zhang, N. Zhang, Z.-R. Tang, Y.-J. Xu, Graphene transforms wide band gap ZnS to a visible light photocatalyst. The new role of graphene as a macromolecular photosensitizer, ACS nano 6 (2012) 9777–9789.
[57] J.M. Coronado, F. Fresno, M.D. Hernández-Alonso, R. Portela, Design of Advanced Photocatalytic Materials for Energy and Environmental Applications, Springer-Verlad, London, 2013.
[58] Z. Li, Z. Xie, Y. Zhang, L. Wu, X. Wang, X. Fu, Wide band gap p-block metal oxyhydroxide InOOH: a new durable photocatalyst for benzene degradation, J. Phys. Chem. C 111 (2007) 18348–18352.